the $2_1^+ \rightarrow 0_1^+$ strength to the sum of all decays from the 0_2^+ level. This ratio is shown in column 3 of Table IV. Although it shows variation from one nucleus to the next, within an order of magnitude the numbers are constant. This is not surprising, since the formation of both levels is due to a complex statistical process, whence large differences in cross sections for exciting analogous levels in neighboring nuclei are not expected. It is somewhat surprising that in Hg^{196} the $0_2^+ \rightarrow 2_1^+$ transition was not seen; that is why only a lower limit is given in column 3 for that nucleus.

The main conclusion that can be reached from the results is that the strengths of the $E0$ transitions from $0_2^+ \rightarrow 0_2^+$ in the nuclei studied are primarily determined by the degree of competition with $E2$ transitions to the first 2^+ level. The general trend in going from Po^{214} to Pt^{194} is to increasing dominance by the latter transition. It may be noted that in a simple vibrational model, the $E0$ transition is forbidden.

In view of the sharp variations with A in the transition-rate ratio found here, it would be interesting to investigate these ratios in other mass regions.

---

*Supported by the National Science Foundation.

†Now at Schlumberger-Doll Research Corporation, Ridgefield, Connecticut 06877.

‡Now at Mobil Research and Development Corporation, Paulsboro, New Jersey 08066.

[1]O. Kofoed-Hansen, J. Lindhard, and O. B. Nielson, Kgl. Danske Videnskab. Selskab, Mat.-Fys. Medd. 25, No. 16 (1950).

[2]T. Yamazaki, E. Matthias, S. G. Prussin, C. M. Lederer, J. Jaclevic, and J. M. Hollander, J. Phys. Soc. Japan Suppl. 24, 167 (1968).

[3]M. Sakai, T. Yamazaki, and H. Ejiri, Nucl. Phys. 74, 81 (1965).

[4]C. M. Lederer, J. M. Hollander, and I. Perlman, Table of Isotopes (John Wiley & Sons, Inc., New York, 1967) 6th ed.

PHYSICAL REVIEW C VOLUME 1, NUMBER 5 MAY 1970

Shell-Model Continuum in Nuclear Bound States

R. H. Ibarra and B. F. Bayman

School of Physics and Astronomy, University of Minnesota, Minneapolis, Minnesota 55455

(Received 10 September 1969)

Shell-model calculations are performed for bound 0^+ states of Ca^{42} and Ni^{58}. The neutron configurations $1f_{7/2}$, $2p_{3/2}$, $2p_{1/2}$, $1f_{5/2}$, and $1g_{9/2}$ are included, as well as states in which one of the neutrons is in the shell-model continuum. These continuum contributions have little effect on energy eigenvalues, but modify the wave functions in the vicinity of the nuclear surface. The calculated wave functions yield one-particle-transfer form factors whose logarithmic derivatives at large radius are consistent with the neutron separation energies. Comparison is made with other procedures for calculating form factors within the framework of the ordinary shell model. It is found that the conventional well-depth procedure underestimates the (p,d) cross sections for populating highly excited states, relative to low-lying states, by about 50%. Two-neutron-transfer cross sections are also calculated and are found to be in agreement with those yielded by the well-depth procedure. However, some of our form factors exhibit an extra node at 8 F, showing that they do not decay like a Hankel function.

I. INTRODUCTION

When we do nuclear shell-model calculations, we have in mind two Hamiltonians: the shell-model Hamiltonian and the "true" Hamiltonian. The true Hamiltonian has a spectrum consisting of discrete states (the bound states of the system) and a continuum (scattering states). If the shell-model potential has finite range and depth, then the shell-model Hamiltonian also has a spectrum with discrete states and a continuum. Shell-model spectroscopic calculations generally attempt to express bound eigenstates of the true Hamiltonian in terms of bound eigenstates of the shell-model Hamiltonian. However, it is clear that an expansion of a bound eigenstate of the true Hamiltonian in terms of eigenstates of the shell-model Hamiltonian, will involve continuum shell-model eigenstates as

well as bound ones.[1] We might expect that the inclusion of these continuum shell-model states will have relatively little effect on the calculated energies of the nuclear bound states, or on the wave functions of the bound states within the nucleus where the shell-model bound-state wave functions are large. However, in the region just beyond the nuclear surface, where the shell-model bound-state wave functions are decreasing exponentially, the shell-model continuum states can make an important contribution.

The aim of this paper is to describe some simple shell-model calculations for nuclear bound states in which the shell-model continuum is included amongst the basis states. The improved wave functions we obtain will be used to calculate cross sections for particle transfer reactions. This will provide a check on some of the prescriptions now in use for calculating form factors.

II. THEORY

We assume that the true nuclear Hamiltonian H can be written

$$H = H_0 + V, \tag{1}$$

$$V = \tfrac{1}{2}\sum_{i\neq j} v(i,j), \tag{2}$$

where H_0 is the shell-model Hamiltonian and V is the residual interaction. Let us denote a discrete eigenstate of H_0 by Φ_α and a continuum eigenstate by $\Phi_{\beta\epsilon}$. Here ϵ is the kinetic energy of the nucleons in the continuum and β characterizes the other nucleons in a bound shell-model state. The set $\{\Phi_\alpha, \Phi_{\beta\epsilon}\}$ forms a complete set of suitably antisymmetrized states in which we attempt to expand ψ_I of H:

$$\psi_I = \sum_\alpha a_\alpha^I \Phi_\alpha + \sum_\beta \int d\epsilon\, a_{\beta\epsilon}^I \Phi_{\beta\epsilon}. \tag{3}$$

Here a_α^I and $a_{\beta\epsilon}^I$ are coefficients to be determined so as to make ψ_I a solution of the Schrödinger equation. If ψ_I is substituted into

$$H\psi_I = E_I\psi_I, \tag{4}$$

and we project this equation onto Φ_α and $\Phi_{\beta\epsilon}$, we get

$$(\epsilon_\alpha - E_I)a_\alpha^I + \sum_{\alpha'}\langle\Phi_\alpha|V|\Phi_{\alpha'}\rangle a_{\alpha'}^I + \sum_{\beta'}\int d\epsilon'\langle\Phi_\alpha|V|\Phi_{\beta'\epsilon'}\rangle a_{\beta'\epsilon'}^I = 0, \tag{5a}$$

$$\sum_{\alpha'}\langle\Phi_{\beta\epsilon}|V|\Phi_{\alpha'}\rangle a_{\alpha'}^I + (\epsilon_\beta + \epsilon - E_I)a_{\beta\epsilon}^I + \sum_{\beta'}\int d\epsilon'\langle\Phi_{\beta\epsilon}|V|\Phi_{\beta'\epsilon'}\rangle a_{\beta'\epsilon'}^I = 0. \tag{5b}$$

We have normalized our shell-model eigenstates as follows:

$$\langle\Phi_\alpha|\Phi_{\alpha'}\rangle = \delta_{\alpha\alpha'}, \tag{6a}$$

$$\langle\Phi_{\beta\epsilon}|\Phi_{\beta'\epsilon'}\rangle = \delta_{\beta\beta'}\delta(\epsilon-\epsilon'). \tag{6b}$$

The coefficients a_α^I and $a_{\beta\epsilon}^I$ are obtained by solving Eq. (5) subject to boundary conditions depending upon whether ψ_I is a bound state or a scattering state.

So far everything has been exact. However, Eq. (5) is an infinite set of coupled integral equations. To do practical calculations we must truncate it. Previous calculations for bound ψ_I have included only Φ_α; we shall also include some states of the set $\Phi_{\beta\epsilon}$. To keep the calculation to a manageable size, we shall follow Bloch[2] in considering only those $\Phi_{\beta\epsilon}$ in which one particle occupies a continuum single-particle shell-model orbit.

The matrix elements in Eq. (5) are calculated in the same way as in the ordinary shell-model calculations except for $\langle\Phi_{\beta\epsilon}|V|\Phi_{\beta'\epsilon'}\rangle$ which requires more consideration. It can easily be shown[2] that this breaks up into two terms:

$$\langle\Phi_{\beta\epsilon}|V|\Phi_{\beta'\epsilon'}\rangle = \langle\Phi_\beta|V_b|\Phi_{\beta'}\rangle\delta(\epsilon-\epsilon') + \langle\Phi_{\beta\epsilon}|V_c|\Phi_{\beta'\epsilon'}\rangle. \tag{7}$$

The first term describes $N-1$ interacting nucleons in bound states, plus one extra nucleon in the continuum that does not interact with the other $N-1$ nucleons. The second term represents the interaction of the nucleon in the continuum with the $N-1$ bound nucleons. Equation (5b) may then be written

$$\sum_{\alpha'}\langle\Phi_{\beta\epsilon}|V|\Phi_{\alpha'}\rangle a_{\alpha'}^I + (\epsilon_\beta+\epsilon-E_I)a_{\beta\epsilon}^I + \sum_{\beta'}\langle\Phi_\beta|V_b|\Phi_{\beta'}\rangle a_{\beta'\epsilon}^I + \sum_{\beta'}\int d\epsilon'\langle\Phi_{\beta\epsilon}|V_c|\Phi_{\beta'\epsilon'}\rangle a_{\beta'\epsilon'}^I = 0. \tag{8}$$

It is convenient to express the continuum states in the basis of reaction-channel states defined in Ref. 2. We write

$$\Phi_{\beta\epsilon} = \sum_\lambda \Phi_{\lambda\epsilon} u_{\beta\lambda}, \tag{9a}$$

$$a_{\beta\epsilon}^I = \sum_\lambda a_{\lambda\epsilon}^I u_{\beta\lambda}, \tag{9b}$$

where the coefficients $u_{\beta\lambda}$ satisfy the eigenvalue equation:

$$(\epsilon_\beta - E_\lambda)u_{\beta\lambda} + \sum_{\beta'}\langle\Phi_\beta|V_b|\Phi_{\beta'}\rangle u_{\beta'\lambda} = 0. \tag{10}$$

Each reaction channel λ describes a possible breakup of the N-nucleon system into one nucleon and a residual nucleus of $N-1$ bound nucleons. In terms

of this new basis for the continuum we get,

$$(\epsilon_\alpha - E_I)a_\alpha^I + \sum_{\alpha'}\langle\Phi_\alpha|V|\Phi_{\alpha'}\rangle a_{\alpha'}^I + \sum_{\lambda'}\int d\epsilon'\langle\Phi_\alpha|V|\Phi_{\lambda'\epsilon'}^I\rangle = 0, \tag{11a}$$

$$\sum_{\alpha'}\langle\Phi_{\lambda\epsilon}|V|\Phi_{\alpha'}\rangle a_{\alpha'}^I + (\epsilon+E_\lambda - E_I)a_{\lambda\epsilon}^I + \sum_{\lambda'}\int d\epsilon'\langle\Phi_{\lambda\epsilon}|V_c|\Phi_{\lambda'\epsilon'}\rangle a_{\lambda'\epsilon'}^I = 0. \tag{11b}$$

These equations contain all the information we want to know about the nuclear system.

2.1 Numerical Treatment of the Continuous Spectrum

We evaluate the energy integrals in Eq. (11) numerically by replacing them by discrete sums over certain given energy values. Then the set of coupled equations can be written

$$\sum_{\alpha'}[(\epsilon_\alpha - E)\delta_{\alpha\alpha'} + \langle\Phi_\alpha|V|\Phi_{\alpha'}\rangle]a_{\alpha'} + \sum_{j,\lambda'}\omega_j\langle\Phi_\alpha|V|\Phi_{\lambda'\epsilon_j}\rangle a_{\lambda'\epsilon_j} = 0, \tag{12a}$$

$$\sum_{\alpha'}\langle\Phi_{\lambda\epsilon_I}|V|\Phi_{\alpha'}\rangle a_{\alpha'} + \sum_{j,\lambda'}[(E_\lambda+\epsilon_I - E)\delta_{\lambda\lambda'}\delta_{ij} + \omega_j\langle\Phi_{\lambda\epsilon_I}|V_c|\Phi_{\lambda'\epsilon_j}\rangle]a_{\lambda'\epsilon_j} = 0, \tag{12b}$$

where the constants ω_j are the weight factors characterizing the chosen method of integration. The system of Eqs. (12) defines a matrix eigenvalue equation. However, it is not ideal for numerical calculations, since the resulting energy matrix that has to be diagonalized is not symmetric. To put it in symmetric form, we have to multiply Eq. (12b) by $\omega_I^{1/2}$. Taking as components of the eigenvector the quantities

$$\tilde{a}_\alpha \equiv a_\alpha, \tag{13a}$$

$$\tilde{a}_{\lambda\epsilon_I} \equiv \omega_I^{1/2} a_{\lambda\epsilon_I}, \tag{13b}$$

and introducing the states

$$\tilde{\Phi}_\alpha \equiv \Phi_\alpha, \tag{14a}$$

$$\tilde{\Phi}_{\lambda\epsilon_I} \equiv \omega_I^{1/2}\Phi_{\lambda\epsilon_I}, \tag{14b}$$

we obtain

$$\sum_{\alpha'}[(\epsilon_\alpha - E)\delta_{\alpha\alpha'} + \langle\tilde{\Phi}_\alpha|V|\tilde{\Phi}_{\alpha'}\rangle]\tilde{a}_{\alpha'} + \sum_{j,\lambda'}\langle\tilde{\Phi}_\alpha|V|\tilde{\Phi}_{\lambda'\epsilon_j}\rangle\tilde{a}_{\lambda'\epsilon_j} = 0, \tag{15a}$$

$$\sum_{\alpha'}\langle\tilde{\Phi}_{\lambda\epsilon_I}|V|\tilde{\Phi}_{\alpha'}\rangle\tilde{a}_{\alpha'} + \sum_{j,\lambda'}[(E_\lambda+\epsilon_I - E)\delta_{\lambda\lambda'}\delta_{ij} + \langle\tilde{\Phi}_{\lambda\epsilon_I}|V_c|\tilde{\Phi}_{\lambda'\epsilon_j}\rangle]\tilde{a}_{\lambda'\epsilon_j} = 0, \tag{15b}$$

or in matrix notation

$$HA = EA, \tag{16}$$

where

$$H = \begin{bmatrix} H_{11} & H_{12} \\ H_{21} & H_{22} \end{bmatrix} \qquad A = \begin{bmatrix} \tilde{a}_\alpha \\ \vdots \\ \tilde{a}_{\lambda\epsilon_I} \end{bmatrix},$$

$$(H_{11})_{\alpha\alpha'} = \langle\tilde{\Phi}_\alpha|V|\tilde{\Phi}_{\alpha'}\rangle + \epsilon_\alpha\delta_{\alpha\alpha'}, \tag{17}$$

$$(H_{12})_{\alpha,\lambda\epsilon_I} = (H_{21})_{\lambda\epsilon_I,\alpha} = \langle\tilde{\Phi}_\alpha|V|\tilde{\Phi}_{\lambda\epsilon_I}\rangle,$$

$$(H_{22})_{\lambda\epsilon_I,\lambda'\epsilon_j} = \langle\Phi_{\lambda\epsilon_I}|V_c|\Phi_{\lambda'\epsilon_j}\rangle + (\epsilon_I+E_\lambda)\delta_{\lambda\lambda'}\delta_{ij}.$$

A determines the wave function of the N-nucleon system

$$\psi = \sum_\alpha \tilde{a}_\alpha\tilde{\Phi}_\alpha + \sum_{I,\lambda}\tilde{a}_{\lambda\epsilon_I}\tilde{\Phi}_{\lambda\epsilon_I}. \tag{18}$$

Note that the continuum states enter exactly in our calculations as the discrete states, except that they carry a weight of $\omega_I^{1/2}$. Equation (16) is the basic equation that we will be using in all our bound-state calculations.

2.2 Application to a Particle in a Square Well

In deriving the matrix eigenvalue equation in (16), we have replaced the integration over the continuous energy variable by a finite sum, the dimension of the matrix being proportional to the number of intervals. It is necessary from the computational point of view to keep the size of this matrix as small as possible. Thus, we have to use integration methods that give fairly good accuracy with a small number of points over a large interval of integration.

To test the possibility of practical calculations in the framework outlined in the preceding section, we have applied the method to an s-state particle bound in a square-well potential utilizing Simpson's integration formula. The purpose of the computational experiment was to study the effects on the accuracy of the solution introduced by varying the upper limit of integration and the integration step size in the energy integrals.

The unperturbed Hamiltonian was taken to be the kinetic energy of the particle and the interaction V was the square well of depth $V_0 = -10$ MeV and radius $R = 4$ F. The configuration states are free particle waves

$$\Phi_\epsilon(r) = (2/\pi\hbar^2 k)^{1/2}\sin(kr), \qquad k = (2\epsilon/\hbar^2)^{1/2}, \tag{19}$$

normalized according to

$$\langle\Phi_\epsilon(r)|\Phi_{\epsilon'}(r)\rangle = \delta(\epsilon - \epsilon'). \tag{20}$$

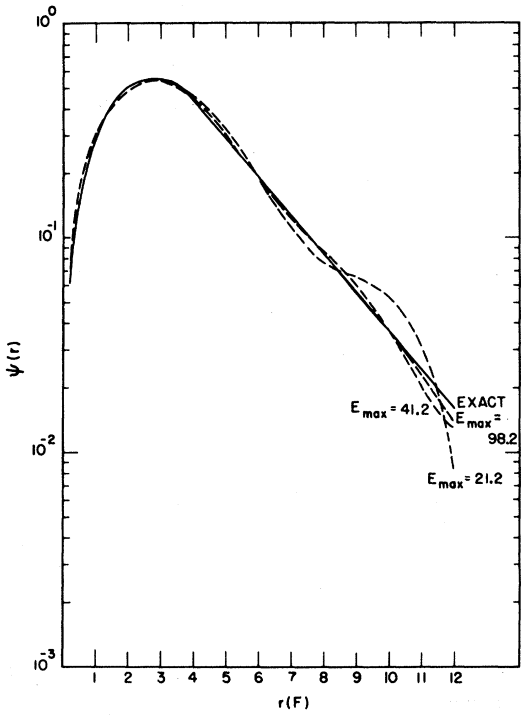

FIG. 1. Influence of the size of configuration space on the accuracy of the solution. For a fixed integration step size (2.5 MeV) the exact solution (solid line curve) is compared to the results (dashed curves) obtained by our formalism for various extensions of E_{max} of the configuration space.

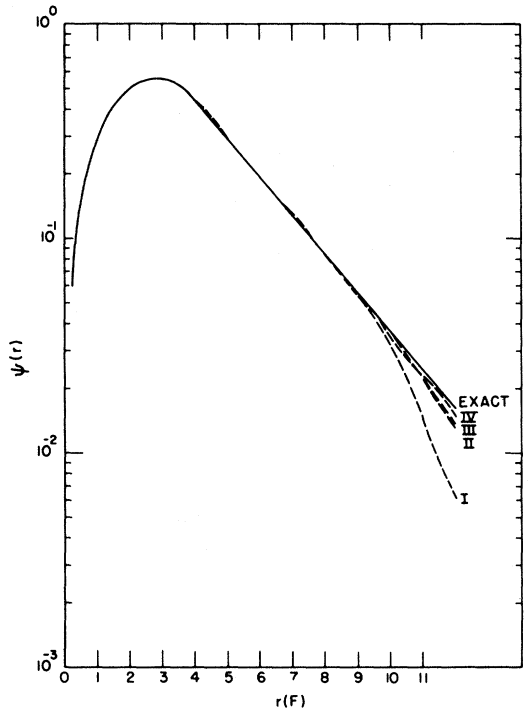

FIG. 2. Influence of the integration step size on the accuracy of the solution. For a fixed E_{max} (98.2 MeV) the integration step lengths used were: 1., 1.5, 2.5, 5.0 for curves I, II, III, IV.

For the well parameters specified above, we get only one bound state. Figure 1 displays the calculated wave functions in comparison with the exact one obtained by an elementary calculation. We have taken into account unperturbed states up to a maximum energy $E_{max} = 21.2$, 41.2, and 98.2 MeV for a fixed integration step size. We see that for small E_{max} the wave function oscillates about the exact solution represented by the solid dark line. These oscillations die down rapidly as E_{max} is increased. There is very good agreement between the calculated wave function and the exact solution for $E_{max} = 98.2$ MeV. No significant change was obtained for E_{max} higher than this value. This indicates that a rather limited configuration space can yield a reasonably accurate solution. The remaining small inaccuracy may be attributed to errors introduced by the integration method and could be minimized by using better integration routines.

The exact energy eigenvalue ($E = -3.592$ MeV) was well approximated by our calculation. For $E_{max} = 21.2$, 41.2, and 98.2 MeV, the calculated energy eigenvalues were −3.470, −3.540, and −3.579 MeV, respectively. This indicates that for calculating energy eigenvalues, it is sufficient to work on a limited set of basis states.

Figure 2 displays the influence of the step size of the integration on the accuracy of the solution. We find that for a smaller number of integration points, the calculated wave function starting at around 8 F falls off more rapidly than the exact solution. On the other hand, the interior part of the solution almost remains the same with respect to variation of integration step sizes. The reduction of the integration step size brings improvement to the accuracy of the solution as indicated by curves I, II, III, and IV.

The results are very encouraging. Better integration methods would allow us to reduce the number of integration points for the same accuracy. The calculation was repeated using the Gaussian quadrature method for the numerical integration. We found that we can achieve better accuracy with only half as many points as were used in Simpson's formula.

3. APPLICATION TO SINGLE-PARTICLE TRANSFER REACTIONS

In this section, a distorted-wave Born-approximation (DWBA) analysis of the $Ca^{42}(p,d)Ca^{41}$ and $Ni^{58}(p,d)Ni^{57}$ reactions is used to study the dependence of the theoretical cross sections upon the nu-

clear wave functions. In particular, we have considered the question of how the interaction of the valence neutrons mixes into the wave functions single-particle states from the continuum, and consider whether the conventional procedure, which emphasizes the asymptotic tail of the form factor, does give a correct measure of the mixing.

$$\psi_0^0(\vec{r}_1\sigma_1,\vec{r}_2\sigma_2)=\sum_{nlj=1f_{7/2},2p_{3/2},2p_{1/2},1f_{5/2}}\Big\{a_{nlj}[\Phi^{nlj}(\vec{r}_1\sigma_1)\Phi^{nlj}(\vec{r}_2\sigma_2)]_0^0 + \int_0^\infty d\epsilon\, a_{\epsilon nlj}\frac{[\Phi^{nlj}(\vec{r}_1\sigma_1)\Phi^{\epsilon lj}(\vec{r}_2\sigma_2)]_0^0-[\Phi^{nlj}(\vec{r}_2\sigma_2)\Phi^{\epsilon lj}(\vec{r}_1\sigma_1)]_0^0}{\sqrt{2}}\Big\} \quad (21)$$

$$\Phi_m^{(\ )lj}(\vec{r}\sigma)=u_{(\ )lj}(r)[Y^l(\hat{r})\chi^{1/2}(\sigma)]_m^j. \quad (22)$$

The a_{nlj} and $a_{\epsilon nlj}$ satisfy the coupled equations

$$(2\epsilon_{nlj}-E)a_{nlj}+\sum_{n'l'j'}\langle[\Phi_{(1)}^{nlj}\Phi_{(2)}^{nlj}]_0^0|v|[\Phi_{(1)}^{n'l'j'}\Phi_{(2)}^{n'l'j'}]_0^0\rangle a_{n'l'j'} + \sum_{n'l'j'}\int_0^\infty d\epsilon'\left\langle[\Phi_{(1)}^{nlj}\Phi_{(2)}^{nlj}]_0^0\left|v\right|\frac{[\Phi_{(1)}^{n'l'j'}\Phi_{(2)}^{\epsilon'l'j'}]_0^0-[\Phi_{(2)}^{n'l'j'}\Phi_{(1)}^{\epsilon'l'j'}]_0^0}{\sqrt{2}}\right\rangle a_{\epsilon'n'l'j'}=0, \quad (23a)$$

$$(\epsilon+\epsilon_{nlj}-E)a_{\epsilon nlj}+\sum_{n'l'j'}\left\langle\frac{[\Phi_{(1)}^{nlj}\Phi_{(2)}^{\epsilon lj}]_0^0-[\Phi_{(2)}^{nlj}\Phi_{(1)}^{\epsilon lj}]_0^0}{\sqrt{2}}\right|v\left|[\Phi_{(1)}^{n'l'j'}\Phi_{(2)}^{n'l'j'}]_0^0\right\rangle a_{n'l'j'} + \sum_{n'l'j'}\int_0^\infty d\epsilon'\left\langle\frac{[\Phi_{(1)}^{nlj}\Phi_{(2)}^{\epsilon lj}]_0^0-[\Phi_{(2)}^{nlj}\Phi_{(1)}^{\epsilon lj}]_0^0}{\sqrt{2}}\right|v\left|\frac{[\Phi_{(1)}^{n'l'j'}\Phi_{(2)}^{\epsilon'l'j'}]_0^0-[\Phi_{(2)}^{n'l'j'}\Phi_{(1)}^{\epsilon'l'j'}]_0^0}{\sqrt{2}}\right\rangle a_{\epsilon'n'l'j'}=0. \quad (23b)$$

The $n'l'j'$ sums correspond to the four states $1f_{7/2}$, $2p_{3/2}$, $2p_{1/2}$, and $1f_{5/2}$.

The core-particle interaction representing the Hartree-Fock self-consistent field was simulated by a Woods-Saxon well

$$V(r)=V_0\left(f(r)-\frac{\lambda\hbar^2}{2m^2c^2}\frac{1}{r}\frac{df}{dr}\vec{s}\cdot\vec{l}\right), \quad (24)$$

$$f(r)=\{1+\exp[(r-r_0A^{1/3})/a_0]\}^{-1}. \quad (25)$$

The well geometry and depth listed in the first row of Table I have been chosen from the requirement that they reproduce as nearly as possible the experimentally observed single-particle energies in Ca^{41} (see Table II), while at the same time fitting the energy of the $1f_{7/2}$ state exactly with the experimentally observed value.

TABLE I. Woods-Saxon well parameters for neutron single-particle states.

Nucleus	V_0 (MeV)	λ	r_0 (F)	a_0 (F)
Ca^{41}	−54.63	19.9	1.24	0.65
Ni^{57}	−53.30	15.	1.25	0.75

3.1 $Ca^{42}(p,d)Ca^{41}$

We represent Ca^{40} as a doubly-closed-shell structure. Then the low-lying states of Ca^{41} are single-particle neutron states, and the ground state of Ca^{42} is a superposition of two-neutron states coupled to zero total angular momentum:

The discrete and continuum single-particle states were calculated by solving the Schrödinger equation with the potential $V(r)$ given above. The continuum shell-model states satisfy δ-function normalization. This is equivalent to the asymptotic behavior

$$u_{\epsilon lj}(r)\underset{r\to\infty}{\sim}(2m/\pi\hbar^2k)^{1/2}[\sin(kr-\tfrac{1}{2}l\pi+\delta_{lj})]/kr, \quad (26)$$

$$k=(2m\epsilon/\hbar^2)^{1/2},$$

where δ_{lj} is the phase shift due to the shell-model potential. The discrete states are normalized in the usual way.

For simplicity, we have used a simple two-body interaction of Gaussian form,

$$v(\vec{r}_1,\vec{r}_2)=v_0\exp(-|\vec{r}_1-\vec{r}_2|^2/\sigma^2), \quad (27)$$

with $v_0=-43.5$ MeV and $\sigma=1.5$ F. The strength of the interaction has been chosen so as to yield the correct Ca^{42} ground-state binding energy. Since our primary objective was to study form factors we made no attempts to investigate whether this

force could give a reasonable description of the low-lying levels of Ca^{42}. The matrix elements of v between two-particle states are simple and are given by

$$\left\langle \frac{[\Phi_{(1)}^{\alpha lj}\Phi_{(2)}^{\beta lj}]_0^0 - [\Phi_{(2)}^{\alpha lj}\Phi_{(1)}^{\beta lj}]_0^0}{[2(1+\delta_{\alpha\beta})]^{1/2}} \middle| v(|\vec{r}_1-\vec{r}_2|) \middle| \frac{[\Phi_{(1)}^{\alpha' l' j'}\Phi_{(2)}^{\beta' l' j'}]_0^0 - [\Phi_{(2)}^{\alpha' l' j'}\Phi_{(1)}^{\beta' l' j'}]_0^0}{[2(1+\delta_{\alpha'\beta'})]^{1/2}} \right\rangle$$
$$= [(2j'+1)/(2j+1)]^{1/2} \sum_k F^k(\alpha\beta lj;\alpha'\beta' l' j')(kj'0\tfrac{1}{2}|j\tfrac{1}{2})^2, \quad (28)$$

where F^k is the generalized Slater integral:

$$F^k(\alpha\beta lj;\alpha'\beta' l' j') = v_0 \int_0^\infty\int_0^\infty \frac{[u_{\alpha lj}(r_1)u_{\beta lj}(r_2)+u_{\alpha lj}(r_2)u_{\beta lj}(r_1)]^*}{[(1+\delta_{\alpha\beta})(1+\delta_{\alpha'\beta'})]^{1/2}} u_{\alpha' l' j'}(r_1)u_{\beta' l' j'}(r_2) f_k(r_1,r_2) r_1^2 r_2^2 dr_1 dr_2, \quad (29)$$

$$f_k(r_1,r_2) = (i)^k(2k+1)\, e^{-(r_1^2+r_2^2)/\sigma^2} j_k\left(\frac{2r_1r_2}{i\sigma^2}\right). \quad (30)$$

As in our test calculation, the number of integration points and maximum energy of integration have been varied to test the convergence of the numerical integration over the energy variable. The Gaussian quadrature technique was used in evaluating the energy integrals because of its better accuracy. This and the fact that the energy integrations involved matrix elements which varied slowly as functions of energy, have allowed us to use an integration step size as large as 10 MeV. A value of 300 MeV for E_{max} gave satisfactory results for the energy integrations. All our calculations were done on the CDC 6600 computer of the University of Minnesota Numerical Analysis Center.

The calculated amplitudes for the different components in the Ca^{42} ground-state wave function are listed in Table III. Also shown are the amplitudes obtained by the usual shell-model calculation that did not include the shell-model continuum states. We see that the wave function from the second calculation contains slightly less $(2p_{3/2}^2)^{0^+}$, $(2p_{1/2}^2)^{0^+}$, and $(1f_{5/2}^2)^{0^+}$ but more $(1f_{7/2}^2)^{0^+}$ than the more "exact" calculation. However the changes are too small to have any significance. We have also shown in Table III the contribution of the continuum states to the wave function. Although their admixtures are small, continuum states have relatively larger amplitudes near the nuclear surface than bound states which then increase their contribution to the cross sections.

The changes in the calculated energies as a result of the introduction of continuum states were quite insignificant. In each case, the observed shift in energy was less than 0.15 MeV.

This completes the nuclear-structure part of the calculation. The form factor for the pickup reaction was calculated by taking the overlap of the Ca^{42} wave function [Eq. (21)] with the single-particle state of Ca^{41}. The resulting expression for the radial form factor $F_{lj}(r)$ is,

$$\frac{F_{lj}(r)}{r} = a_{nlj}u_{nlj}(r) + \frac{1}{\sqrt{2}}\int_0^\infty d\epsilon\, a_{\epsilon nlj}(r). \quad (31)$$

In the discussion that follows, the "exact" form factor refers to $F_{lj}(r)$ given by Eq. (31), using the a_{nlj} and $a_{\epsilon nlj}$ obtained by solving the set of Eqs. (23).

TABLE II. Single-particle energies in Ca^{41} and Ni^{57} in MeV.

Nucleus	Level	Calculated	Experimental
Ca^{41}	$1f_{7/2}$	−8.361	−8.361
	$2p_{3/2}$	−5.483	−6.291
	$2p_{1/2}$	−3.859	−4.231
	$1f_{5/2}$	−2.782	−2.861
Ni^{57}	$2p_{3/2}$	−10.25	−10.25
	$1f_{5/2}$	−9.64	−9.47
	$2p_{1/2}$	−9.17	−9.17

TABLE III. Configuration mixing amplitudes in the ground-state wave function of Ca^{42}.

Configuration	"Exact" calculation	Ordinary shell model calculation
$(1f_{7/2}^2)^{0^+}$	0.989	0.991
$(1f_{5/2}^2)^{0^+}$	0.0828	0.0807
$(2p_{3/2}^2)^{0^+}$	0.1024	0.1021
$(2p_{1/2}^2)^{0^+}$	0.0406	0.0404
$(1f_{7/2}\epsilon f_{7/2})^{0^+}$	0.0518	...
$(1f_{5/2}\epsilon f_{5/2})^{0^+}$	0.0151	...
$(2p_{3/2}\epsilon p_{3/2})^{0^+}$	0.0259	...
$(2p_{1/2}\epsilon p_{1/2})^{0^+}$	0.0144	...

If use is made of Eqs. (23) and the completeness relation

$$\sum_n u^*_{n\,lj}(r_2)u_{n\,lj}(r_1)+\int_0^\infty d\epsilon\, u^*_{\epsilon\,lj}(r_2)u_{\epsilon\,lj}(r_1)=\frac{\delta(r_2-r_1)}{r_1^{\,2}}, \tag{32}$$

then it can be shown that $F_{lj}(r)$ of Eq. (31) satisfies the differential equation

$$\left[\frac{-\hbar^2}{2m}\left(\frac{d^2}{dr^2}-\frac{l(l+1)}{r^2}\right)+V(r)+\epsilon_{n\,lj}-E\right]F_{lj}(r)$$

$$=-\sum_{\sigma_1,\sigma} r\iint d\vec{r}_1 d\hat{r}\,[\Phi^{n\,lj}(\vec{r}_1\sigma_1)\,\mathcal{Y}^{lj}(\hat{r}\sigma)]^{0*}_0 v(|\vec{r}_1-\vec{r}\,|)\psi^0_0(\vec{r}_1\sigma_1,\vec{r}\sigma)$$

$$+\sum_{\substack{n''\\(n''\neq n)}} ru_{n''lj}(r)\sum_{\sigma_1,\sigma_2}\iint d\vec{r}_1 d\vec{r}_2[\Phi^{n\,lj}(\vec{r}_1\sigma_1)\Phi^{n''lj}(\vec{r}_2\sigma_2)]^{0*}_0 v(|\vec{r}_1-\vec{r}_2|)\psi^0_0(\vec{r}_1\sigma_1,\vec{r}_2\sigma_2)\,. \tag{33}$$

Here ψ^0_0 is the "exact" two-particle wave function, Eq. (21). The n'' sum in the second term on the right-hand side of Eq. (33) extends over all bound lj states except nlj. For example, if nlj refers to $2p_{3/2}$, then $n''lj$ takes on the single value $1p_{3/2}$. If $F_{p_{3/2}}(r)$ were obtained by solving Eq. (33) without the $u_{1p_{3/2}}$ term on the right-hand side, then this $F_{p_{3/2}}(r)$ would not be orthogonal to $u_{1p_{3/2}}(r)$. This would be inconsistent with out assumption that the $1p_{3/2}$ neutron shell is full in both Ca^{42} and Ca^{40}. If nlj refers to $1f_{7/2}$, then there are no $n''lj$ terms on the right-hand side of Eq. (33).

Prakash and Austern[3] and Philpott, Pinkston, and Satchler[4] have worked with an approximate version of Eq. (33) in which: (a) the n'' sum is neglected, (b) the exact wave function ψ^0_0 on the right-hand side of Eq. (33) is replaced by an approximate wave function obtained from a shell-model calculation. In the framework of our discussion, this would correspond to including only the bound-state terms in the expression ψ^0_0 for Eq. (21).

The form factors given by the Prakash-Austern method provide a good approximation to our (more exact) form factors. This will be seen below in our discussion of the $Ni^{58}(p,d)$ reaction. Theirs is a much quicker calculation than ours, and so will be more useful for generating comparisons with experimental data on one-particle transfer reactions. Our method has the advantage that it provides us with an explicit two-particle wave function, which can be used for the calculation of form factors for two-particle transfer reactions (see Sec. 4).

The results of the form-factor calculations are summarized in Figs. 3–6. Radial functions derived in the spirit of ordinary shell-model theory are denoted by (OSM). In this approximation, the form factor is proportional to the single-particle radial wave function, calculated in a fixed shell-model potential. This generally leads to a form factor whose logarithmic derivative beyond the nuclear surface is inconsistent with the neutron separation energy. However, within the nucleus the OSM and exact form factors are similar.

The well-depth (WD) form factors were derived by adjusting the depth of the Woods-Saxon potential in the single-particle Schrödinger equation until the shell-model radial function has the correct logarithmic derivative at large r. The spectroscopic amplitudes that multiplied these radial functions were those determined from the ordinary shell-model calculation without the continuum. They were approximately equal to the amplitudes derived from the normalization of our exact form factors. In order to indicate how much the depth had to be varied to give the underlying state the right asymptotic behavior, we have listed in Table

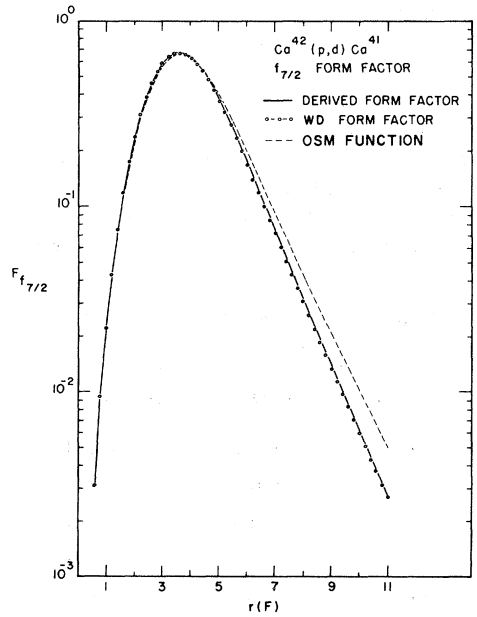

FIG. 3. Pickup form factors for $Ca^{42}(p,d)Ca^{41}$. Our $f_{7/2}$ form factor (solid line curve) is compared with the WD form factor and the OSM radial function.

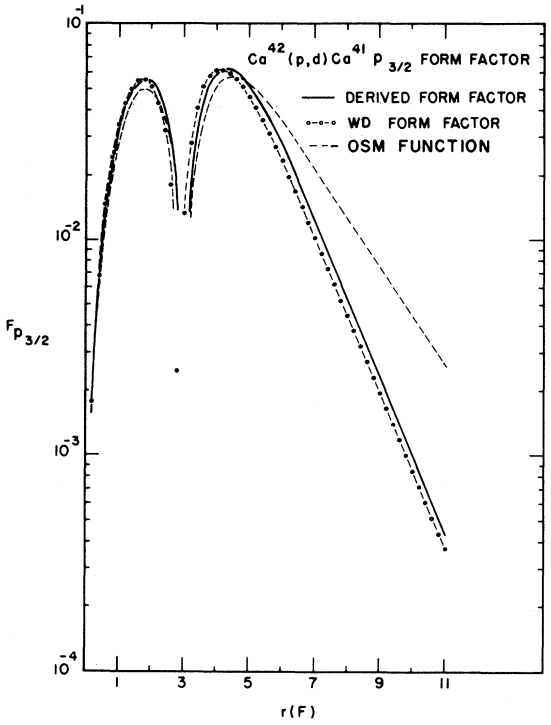

FIG. 4. Pickup form factors for $Ca^{42}(p,d)Ca^{41}$. Our $p_{3/2}$ form factor (solid line curve) is compared with the WD form factor and the OSM radial function.

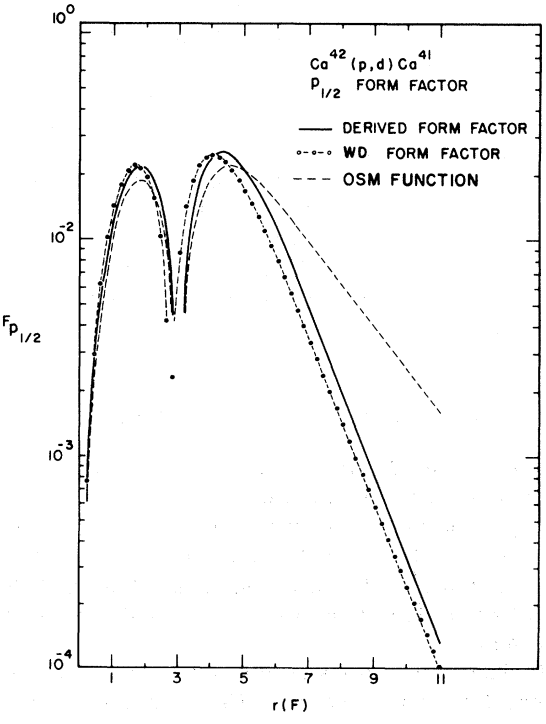

FIG. 5. Pickup form factors for $Ca^{42}(p,d)Ca^{41}$. Our $p_{1/2}$ form factor (solid line curve) is compared with the WD form factor and the OSM radial function.

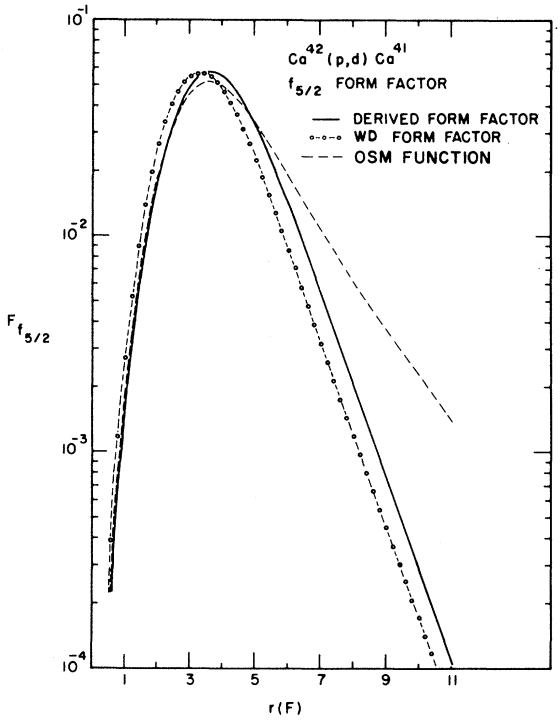

FIG. 6. Pickup form factors for $Ca^{42}(p,d)Ca^{41}$. Our $f_{5/2}$ form factor (solid line curve) is compared with the WD form factor and the OSM radial function.

IV the depths needed to calculate the WD form factors.

An important result in the comparison of the theoretical form factors is the observation that the WD form-factor peaks at a slightly smaller radius than our exact form factor and consequently is smaller in the surface region. This is characteristic of cases for which the separation energy exceeds the single-particle energy of the orbit and is most frequently met in pickup reactions, particularly in going through its small components.[5] This behavior explains the features seen in Fig. 7 which compares angular distributions using our exact form factors and the WD form factors. The distorted-wave calculations were done for 26.5-MeV protons in the zero-range DWBA code of Smith using the optical parameters[6] listed in Table V. For

TABLE IV. Depths of Woods-Saxon wells used to calculate WD form factors ($r_0 = 1.25$ F, $a_0 = 0.65$ F, $\lambda = 19.9$).

Level	Calculated separation energy (MeV)	V_0 (MeV)
$f_{7/2}$	11.47	59.21
$f_{5/2}$	17.04	77.69
$p_{3/2}$	14.34	69.63
$p_{1/2}$	15.97	76.20

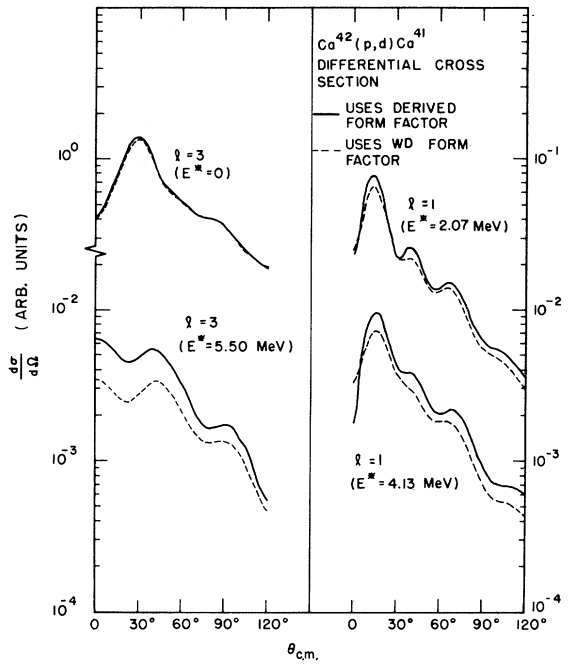

FIG. 7. Comparison of the $Ca^{42}(p,d)Ca^{41}$ angular distributions for the $f_{7/2}$, $p_{3/2}$, $p_{1/2}$, $f_{5/2}$ pickup obtained from our form factors and the WD form factors. The optical parameters are given in Table V.

the $1f_{7/2}$ pickup, our exact form factor was well reproduced by the WD procedure, and no significant change was observed in the cross section. This is understandable since $(1f_{7/2}{}^2)^{0^+}$ is the major component in the ground-state wave function of Ca^{42}, and a single-particle description would be a good approximation. However, for transitions to the excited states, our theory predicted a much larger magnitude for the form factors in the surface region than those predicted by the WD procedure, thus increasing the predicted cross sections by significant amounts. The calculation indicates that well-depth form factors underestimate, by about 50%, the cross sections for populating highly excited single-particle states compared with the ground state.

The transition to the $\frac{7}{2}^-$ ground state of Ca^{41} has been observed in the $Ca^{42}(p,d)Ca^{41}$ reaction by Smith, Bernstein, and Rickey.[6] It was found that the well-depth procedure can give a good account

TABLE V. Proton and deuteron optical parameters. $Ca^{42}(p,d)Ca^{41}$ ($E_p = 26.5$ MeV).

	V (MeV)	W_S (MeV)	r_0 (F)	a_0 (F)	$(r_0)_S$ (F)	$(a_0)_S$ (F)
p	47.6	5.679	1.117	0.69	1.229	0.751
d	116.8	15.7	0.997	0.787	1.422	0.579

of the angular distribution provided the finite-range[7] DWBA code is used. However, nothing has been found which might correspond to the excited single-particle states of Ca^{41}. This is rather unfortunate, because this is where our findings differ from the predictions of the well-depth procedure. Further experimental exploration would therefore, be interesting, since this would be a good testing ground for the theory.

3.2 $Ni^{58}(p,d)Ni^{57}$ $(5/2^-)$

The $\frac{5}{2}^-$ transition is particularly interesting because it exhibits a peculiar angular distribution that cannot be explained by the standard DWBA calculation.[8,9] The experimental angular distribution (see Fig. 10) for the neutron pickup leading to the 0.78-MeV $\frac{5}{2}^-$ level of Ni^{57} shows a more rapid fall-off beyond the first maximum than that given by the DWBA calculation with the well-depth form factor. Prakash and Austern[3] have shown that agreement with experiment is improved if configuration mixing effects are included in the form-factor calculation. We will now apply our method to this case.

We consider Ni^{58} as a doubly closed shell structure plus two neutrons paired off to zero total angular momentum in the unoccupied orbits $2p_{3/2}$, $1f_{5/2}$, $2p_{1/2}$, $1g_{9/2}$, and the single-particle continuum states. The well parameters that were used to calculate these shell-model states are tabulated in the second row of Table I. This potential reproduces closely the single-particle levels of Ni^{57}, including the spin-orbit splitting of the $2p_{3/2}$ and $2p_{1/2}$ levels. However, it is not possible to fit all the single-particle levels exactly with the same potential (see Table II). The depth needed for the $1f_{5/2}$ level is somewhat different from that for the levels $2p_{3/2}$ and $2p_{1/2}$. The difference is, however, small and was ignored in the calculations.

The two-body interaction was taken from the Prakash-Austern paper:

$$v(1,2) = v_0 e^{-|\vec{r}_1-\vec{r}_2|^2/\sigma^2}(P_S + \omega_0 P_t), \qquad (34)$$

$$\omega_0 = 0.5, \quad \sigma = 1.85 \text{ F}, \quad v_0 = 27.5 \text{ MeV}.$$

The operators P_S and P_t project the singlet and triplet components of the wave function, respectively. The value used for v_0 was obtained by requiring that the calculated ground-state energy of Ni^{58} agreed with the observed value. Note that this is a little different from the value used by Prakash and Austern.

Pickup form factors resulting from the various prescriptions are shown in Fig. 8. Again we observe that for large radial distance our form factor lies above the well-depth form factor, but always parallel to it, indicating the internal consis-

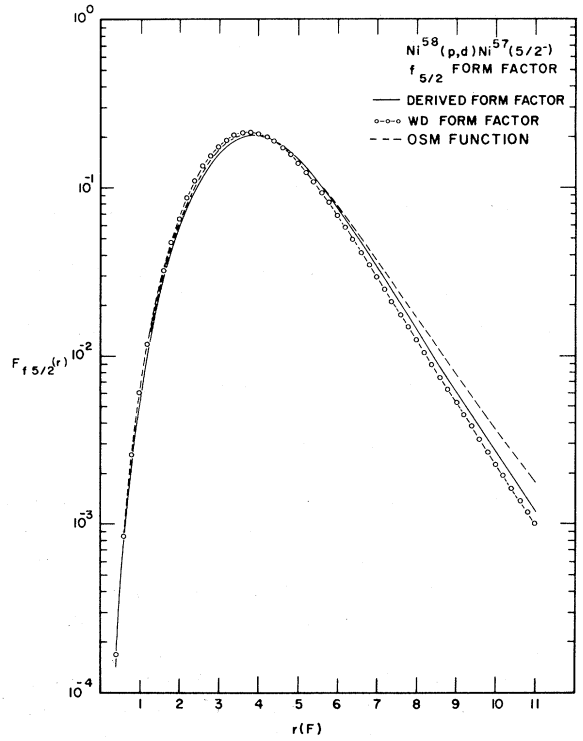

FIG. 8. Pickup form factor for $Ni^{58}(p,d)Ni^{57}$ $(\frac{5}{2}^-)$. The exact form factor (solid line curve) is compared with the WD form factor and the OSM radial function.

tency of our theory. The magnitude of our form factor, in the tail region, is about 25% larger than that of the WD form factor which resulted in a large increase in the magnitude of the cross section. The OSM radial function is also shown for

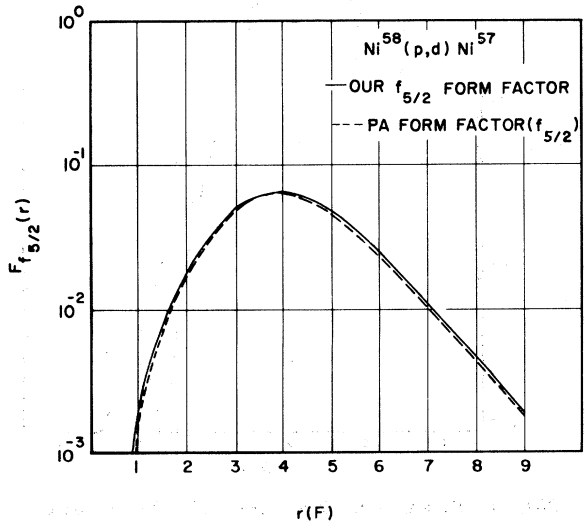

FIG. 9. Comparison of our $f_{5/2}$ form factor with the Prakash-Austern form factor.

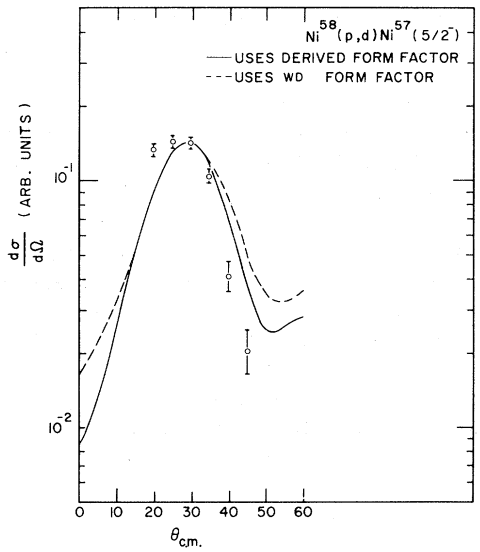

FIG. 10. Peak-to-peak comparison of the $Ni^{58}(p,d)Ni^{57}$ $(\frac{5}{2}^-)$ angular distributions given by our form factor and the WD form factor. The experimental points (open circles) are from Ref. 9. The optical parameters are listed in Table VI.

comparison and again displays the wrong asymptotic form.

Figure 9 shows how the Prakash-Austern approximation to the $f_{5/2}$ form factor compares with our "exact" form factor. The curves are normalized[10] so as to agree at 4 F. It is seen that the Prakash-Austern approximation gives a good representation of the shape of the form factor over the entire calculated range.

Finally, Fig. 10 shows a comparison of our theoretical $f_{5/2}$ angular distribution with that of the well-depth method for the optical parameters in Table VI. The curves are normalized arbitrarily. We find that our curve has moved a good way down from the well-depth curve towards the experimental curve.[9] The improvement in the calculation is comparable to that obtained by the Prakash-Austern calculation.

3.3 Varying the Well Radius as well as the Well Depth

In the WD procedure, the depth of the single-particle well is varied, but its geometry is kept fixed. The variation of the depth of the well is supposed

TABLE VI. Proton and deuteron optical parameters. $Ni^{58}(p,d)Ni^{57}$ ($E_p = 28$ MeV).

	V (MeV)	W_S (MeV)	r_0 (F)	a_0 (F)	$(r_0)_S$ (F)	$(a_0)_S$ (F)
p	44.6	17.1	1.30	0.458	1.070	0.341
d	91.0	18.75	1.15	0.68	1.340	0.680

to reflect the way the valence nucleons cause the separation energy to deviate from the single-particle shell-model energy. It has been pointed out by Austern[11] and by Pinkston and Satchler[12] that the valence nucleons should also change the radius of the effective well. Thus, one could use methods in which the well depth is kept fixed, but the radius is varied until the single-particle binding energy equals the separation energy. Or perhaps both the depth and radius should be varied simultaneously.

Table VII shows some choices for well depths and radii which yield well-depth form factors that agree with our exact form factors. The fact that the effective radius is larger than the single-particle radius is consistent with the arguments of Austern and of Pinkston and Satchler. Of course the numbers in Table VII are not unique; other combinations of well depth, radius and diffuseness would do just as well. Unfortunately, we were unable to find a general radius-plus-depth variation prescription that would always yield a well-depth form factor in agreement with our exact one.

4. APPLICATION TO TWO-PARTICLE TRANSFER REACTIONS

By limiting our attention to the study of single-neutron transfer reactions we have considered only a very small part of the Ca^{42} wave function. To study it further, we have used it to predict the differential cross sections for the 0^+ to 0^+ transitions in the $Ca^{42}(p,t)Ca^{40}$ reaction and its inverse process, $Ca^{40}(t,p)Ca^{42}$.

The radial form factor for an $L=0$ transfer of two neutrons (see Ref. 13) is given by

$$F_0(R) = R\sum_{lj}((l\tfrac{1}{2})_j(l\tfrac{1}{2})_j|(ll)_0(\tfrac{1}{2}\tfrac{1}{2})_0)_0 \times\int d\vec{r}\, e^{-(3/2)\kappa r^2} u_{lj}(r_1,r_2)[Y^l(\hat{r}_1)Y^l(\hat{r}_2)]^0_0, \quad (35)$$

$$\vec{r}_1=\vec{R}-\tfrac{1}{2}\vec{r}, \quad \vec{r}_2=\vec{R}+\tfrac{1}{2}\vec{r},$$

where

$$u_{lj}(r_1,r_2) = \langle\{[Y^l(\hat{r}_1)x^{1/2}(\sigma_1)]^j \times[Y^l(\hat{r}_2)x^{1/2}(\sigma_2)]^j\}^0_0|\psi^0_0(\vec{r}_1,\vec{r}_2)\rangle. \quad (36)$$

TABLE VII. Results of a search for equivalent Woods-Saxon potentials that give correct form factors for $Ca^{42}(p,d)Ca^{41}$ ($\lambda=19.9$, $a_0=0.65$ F).

	V_0 (MeV)	r_0 (F)
$f_{5/2}$	−62.40	1.42
$p_{3/2}$	−64.02	1.32
$p_{1/2}$	−66.12	1.37
S.P. Well	−54.63	1.24

The orbital part of the triton wave function was assumed to be of Gaussian form:

$$\Phi_t(\vec{r}_1,\vec{r}_2,\vec{r}_3) = (216\kappa^6/\pi^3)^{1/2}\exp[-\kappa(|\vec{r}_1-\vec{r}_p|^2 + |\vec{r}_2-\vec{r}_p|^2+|\vec{r}_1-\vec{r}_2|^2)]. \quad (37)$$

A value of $\kappa=0.24$ F^{-2} was used. This is equivalent to taking the triton mean squared radius to be $(1.7\text{ F})^2$.

Equation (35) was evaluated by using a technique developed by Bayman and Kallio[13] for performing integrals of this type with arbitrary two-particle radial functions $u_{lj}(r_1,r_2)$ without resorting to the Talmi-Moshinsky transformations to relative and center-of-mass coordinates.

Figure 11 displays the theoretical form factor for the $Ca^{42}(p,t)Ca^{40}$ reaction predicted by using our nuclear wave function. This is represented by the solid dark line. The ordinary shell-model and well-depth curves were calculated on the assumption that the wave function of the transferred neutrons was a linear combination of shell-model bound-state components: $(1f_{7/2}{}^2)^{0^+}$, $(2p_{3/2}{}^2)^{0^+}$, $(2p_{1/2}{}^2)^{0^+}$, and $(1f_{5/2}{}^2)^{0^+}$. The expansion coefficients listed in the third column of Table III were calculated by diagonalizing the Hamiltonian in this truncated basis. In the ordinary shell-model case all

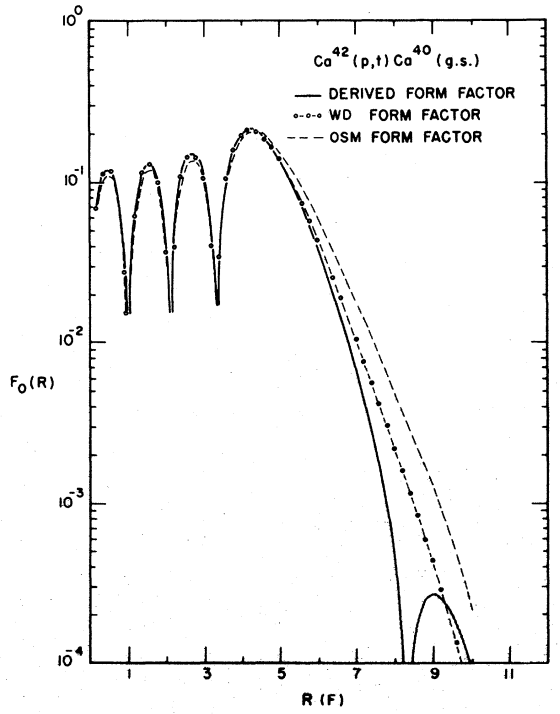

FIG. 11. Pickup form factor for an $L=0$ transfer of two neutrons in $Ca^{42}(p,t)Ca^{40}$. The exact form factor (solid line curve) is compared with the WD form factor and the OSM form factor.

the shell-model states were calculated in the same well with depth $V_0 = -54.63$ MeV. In the well-depth case, a different depth was used for each single-particle state; it was chosen to give each single-particle state a binding energy equal to half the two-neutron separation energy.

The form factors depicted in Fig. 11 have different behavior near the nuclear surface. Asymptotically, the WD form factor displays the Hankel-function decay of a state bound with an energy of −19.833 MeV. Being more deeply bound, it is pulled inwards with respect to the OSM curve. The form factor generated by our wave function is characterized by a rapid falloff punctuated by the presence of an extra node at about 8 F. This is due to the continuum-state admixtures in the wave function which interfere destructively with the discrete configruations at the surface region. This is shown explicitly in Fig. 12 which displays the partial form factors. Except for the $f_{7/2}$ component, all have essentially the same shape as that of the total form factor. The interference effect here is more pronounced than for the case of the single-particle transfer reactions. It is also worth noting that in all but possibly the $f_{5/2}$ partial form factor, the well-depth procedure provides a better approximation to the derived form factor than the ordinary shell-model method. This feature is carried over to the total form factor as is apparent in Fig. 11. The results then strongly favor the use of the well-depth procedure for "everyday" use in existing two-particle transfer codes. This disagrees with the conclusion of Jaffe and Gerace.[14]

Figure 13 shows a comparison between the experimental[15] and the calculated angular distributions. The optical parameters[16] used are listed in Table VIII. The data points were normalized to the calculated curve corresponding to our form factor so as to produce the best visual fit. It is apparent that the extra node in our form factor at 8 F has very little effect on the calculated angular distribution. This is because it occurs in a region where the form factor is very small. The magnitudes of the cross sections are 2.5 : 2.2 : 4.4 for the derived, well-depth, and ordinary shell-model form factors, respectively. However, there is no significant difference in the shape of the calculated angular distributions. This is unfortunate because it becomes impossible to choose among the three wave functions on the basis of shape alone. It is evident that the angular distribution is well reproduced by the three curves. Indeed, the fits are better than one could reasonably expect from a theory that makes crude assumptions about the re-

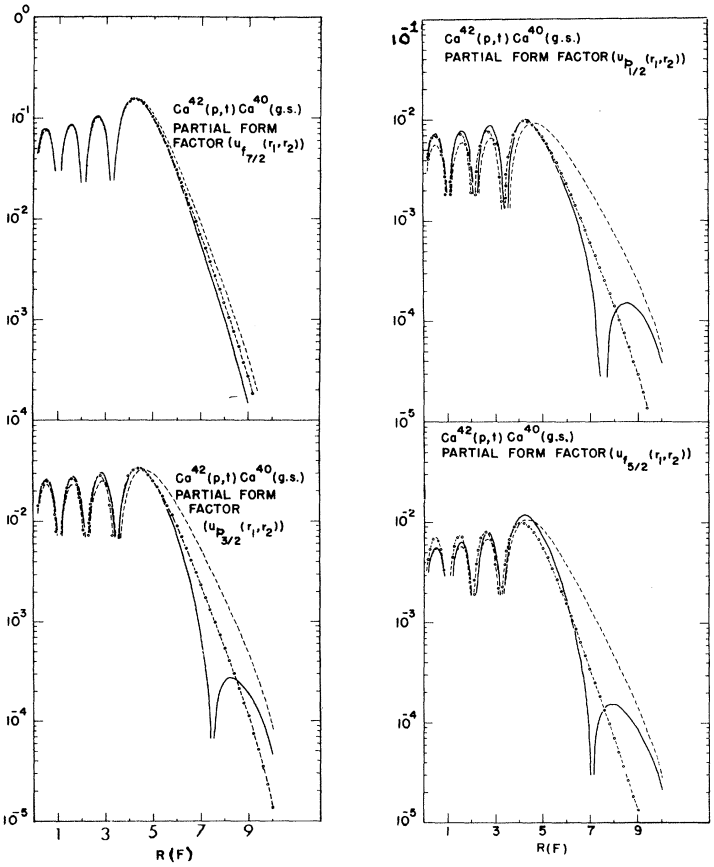

FIG. 12. Components of the form factor for an $L = 0$ transfer of two neutrons in $Ca^{42}(p,t)Ca^{40}$. The sum of these partial form factors gives the (net) form factor dipicted in Fig. 11. ——, derived form factor; .—.—.—., WD form factor; ---, OSM form factor.

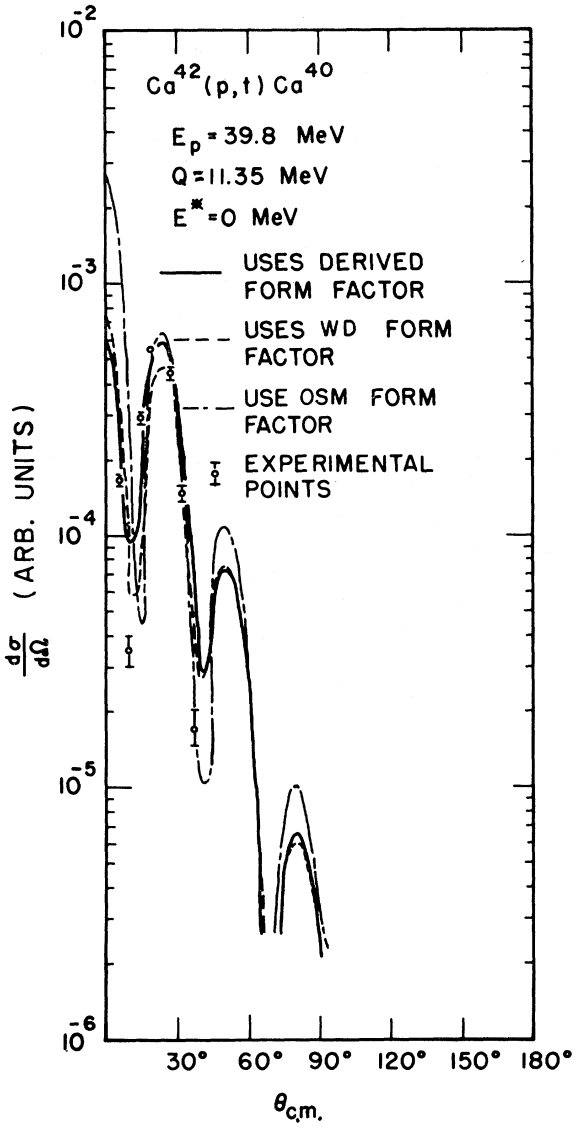

FIG. 13. Comparison between the experimental (open circles) and the calculated angular distributions for the $Ca^{42}(p,t)Ca^{40}$. The optical parameters are listed in Table VIII.

action mechanism.

The computations described above were duplicated for the inverse process $Ca^{40}(t,p)Ca^{42}$ with 12-MeV tritons, using the optical parameters tabulated in Table IX. The results obtained are similar to the (p,t) reaction and are, therefore, not presented in detail here. Figures 14 and 15 summarize the findings. As in the (p,t) reaction, there is not much difference between the theoretical angular distributions except for the magnitudes.

The Ca^{42} 0^+ state at 5.85-MeV excitation energy is probably the one which should be associated with our calculated excited bound state. However, it is observed to be populated in the (t,p) reaction with a strength of only 0.97 that of the ground state, compared to our calculated value of 6.8. The well-depth procedure gives a ratio of 7.7 as compared to 5.5 for the ordinary shell-model method. Our calculated ratio would be decreased if we had more configuration mixing, since more $(2p_{3/2}{}^2)^{0^+}$ admixed into the ground-state would give constructive interference which would enhance the ground-state transition, whereas more $(1f_{7/2}{}^2)^{0^+}$ mixed into the excited state would increase the destructive interference which would retard the excited-state transition. This would indicate that the interaction we used underestimates the amount of configuration mixing. However, increasing the strength of the interaction overpredicts the binding energy of the Ca^{42} ground state. This suggests using a more realistic type of interaction with exchange terms.

The presence of the form factor node at 8 F confirms the argument of Jaffe and Gerace that there is no reason why the form factor should decay like a Hankel function beyond the nuclear surface. A crude explanation of the occurrence of this node is that by including the f-p continuum, we are essentially including contributions from the $2f$-$3p$ oscillator shell. Since a wave function like $(2p_{3/2}\ 3p_{3/2})^{0^+}$ has eight oscillator quanta, it should lead to a form factor that looks like a $5s$ wave function, whereas the six-quanta state $(2p_{3/2}\ 2p_{3/2})^{0^+}$ leads to a 0^+ form factor that looks like a $4s$ wave function. If they start out at $R = 0$ with the same sign, the $4s$ and $5s$ wave functions will have opposite sign at large R, and the $5s$ component will eventually dominate over the $4s$ component, even if the amplitude of the $5s$ component in the form factor is small. Of course, the true wave function will also have components like $(3p_{3/2}\ 3p_{3/2})^{0^+}$ with ten quanta, which will yield a form factor looking like a $6s$ wave function. This has the same sign at

TABLE VIII. Proton and triton optical parameters. $Ca^{42}(p,t)Ca^{40}$ ($E_p = 39.8$ MeV).

	r_0 (F)	a_0 (F)	V (MeV)	$(r_0)_V$ (F)	$(a_0)_V$ (F)	W_V (MeV)	$(r_0)_S$ (F)	$(a_0)_S$ (F)	W_S (MeV)
p	1.18	0.7	43.3	1.3	0.6	2.	1.3	0.6	5.
t	1.24	0.678	146.	1.45	0.841	25.1	...	...	...

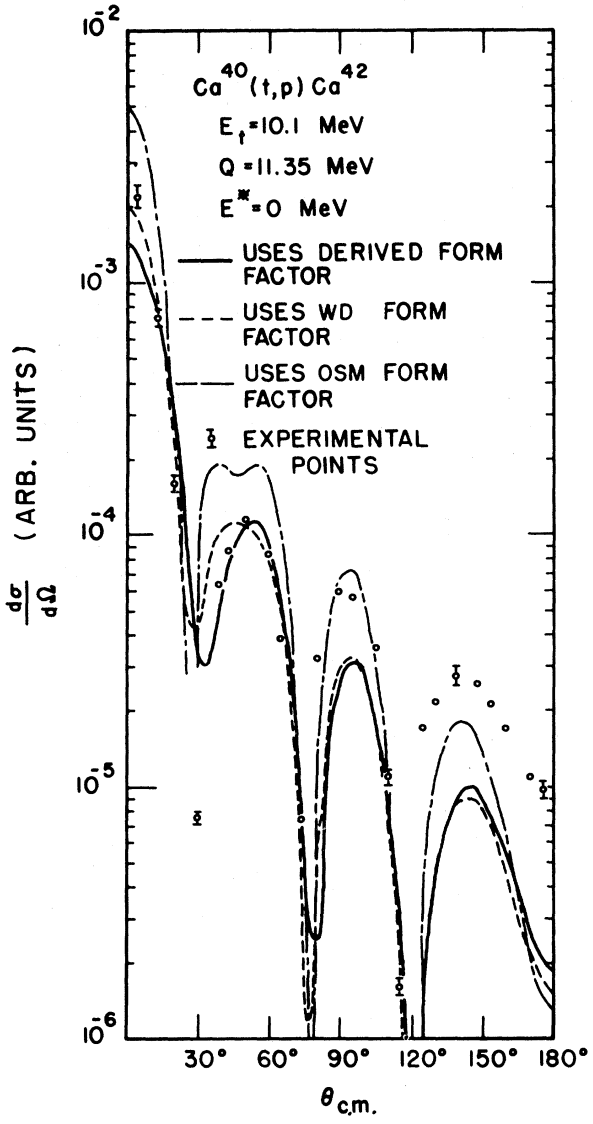

FIG. 14. Comparison between the experimental (open circles) and the calculated angular distributions for the $Ca^{40}(t,p)Ca^{42}$ to the ground state. The optical parameters are listed in Table IX.

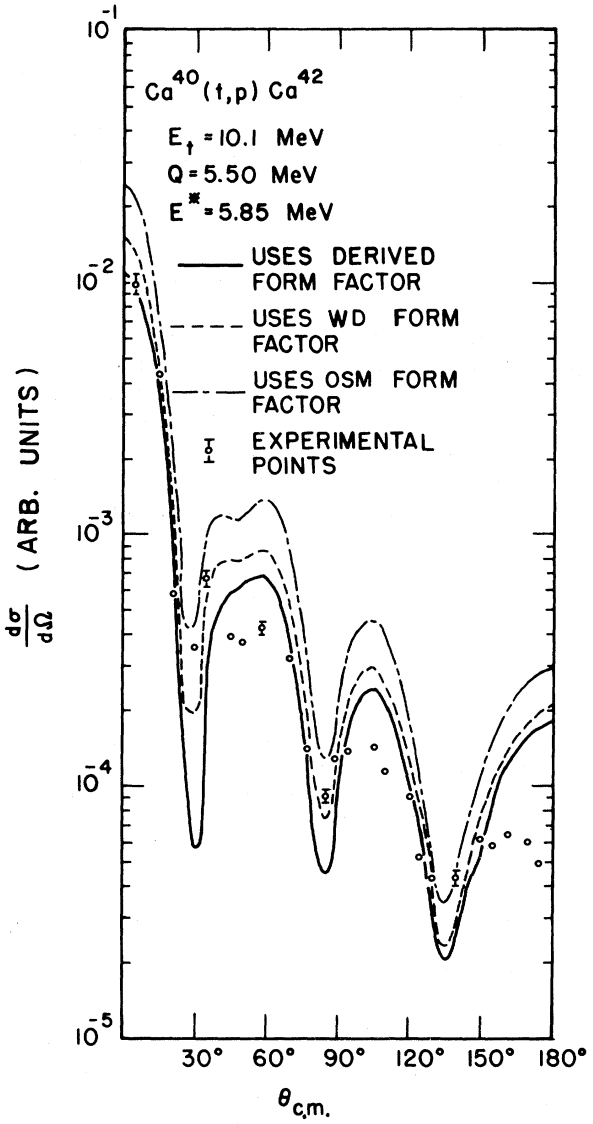

FIG. 15. Comparison between the experimental (open circles) and the calculated angular distributions for the $Ca^{40}(t,p)Ca^{42}$ to the 5.85-MeV 0^+ excited state. The optical parameters are listed in Table IX.

large R as a $4s$ wave function, which makes it unclear whether there is a range in which the opposite sign of the $5s$ wave function can dominate. Since we have only allowed one particle to be in the continuum, our wave function does not have a component like $(3p_{3/2}\,3p_{3/2})^{0^+}$. However, we have estimated its effect in perturbation theory, and our conclusion is that it does not do away with the extra node. Therefore we believe that the node in the ground-state form factor at about 8 F is genuine.

TABLE IX. Proton and triton optical parameters. $Ca^{42}(t,p)Ca^{42}$ ($E_t = 12$ MeV).

	r_0 (F)	a_0 (F)	V (MeV)	$(r_0)_V$ (F)	$(a_0)_V$ (F)	W_V (MeV)	$(r_0)_S$ (F)	$(a_0)_S$ (F)	W_S (MeV)
p	1.25	0.65	53.	...	...	...	1.25	0.47	15.5
t	1.24	0.678	144.	1.45	0.841	30.	...	...	...

5. DISCUSSION

In this work we have attempted to generalize the ordinary shell-model for nuclear bound states by including the continuum spectrum of a realistic shell-model potential. This provided a very direct way to treat binding-energy effects on particle-transfer form factors. We have found that the well-depth procedure tends to underestimate by about 50% the cross sections for populating highly excited single-particle states, compared to the ground state. The Prakash-Austern procedure provides a reasonable approximation to the shape of our more exact form factors. We have also found that versions of the well-depth method in which both the depth and radius of the well are varied provide a better account of the form factors. However, we have not succeeded in finding a unique prescription for the way these two parameters should be varied. Our calculated two-particle-transfer cross sections are closer to the predictions of the well-depth method than to those of the ordinary shell-model method. However, our form factor exhibits an extra node at about 8 F, which shows that it does not decay like a Hankel function beyond the nuclear surface.

The method proposed here for the unbound configurations is an obvious extension of the diagonalization procedure used for discrete configurations. Like the ordinary shell-model formulation it is free from the difficulties associated with antisymmetrization and boundary conditions usually encountered in other formulations. However, the main drawback in the formalism is our failure to include continuum contribution involving more than one particle in the continuum. We have made a preliminary study of this question using perturbation techniques, and the results seem to indicate that admixtures of the double continuum states have very little effect on the calculated form factors. However, this is not a general statement and requires more study.

---

*Work partly based on the Ph.D. thesis of R. H. Ibarra at the University of Minnesota, Minneapolis, Minnesota.

[1]A simple example of a bound state of one Hamiltonian expanded in terms of continuum states of another one is the Fourier transform of a harmonic-oscillator eigenfunction.

[2]C. Bloch, in Many-Body Description of Nuclear Structure and Reactions, Proceedings of the International School of Physics "Enrico Fermi," Course XXXVI, 1966, edited by C. Bloch (Academic Press Inc., New York, 1966).

[3]A. Prakash and N. Austern, Ann. Phys. (N.Y.) 51, 418 (1969).

[4]R. Philpott, W. Pinkston, and G. Satchler, Nucl. Phys. A119, 241 (1968); A125, 176 (1969).

[5]A more detailed discussion of this behavior is given by Philpott, Pinkston, and Satchler, Ref. 4.

[6]S. M. Smith, A. M. Bernstein, and M. E. Rickey, Nucl. Phys. 113, 303 (1968).

[7]The use of this realistic model does not alter our calculation of the nuclear overlaps.

[8]E. Rost, B. F. Bayman, and R. Sherr, Bull. Am. Phys. Soc. 9, 458 (1964).

[9]R. Sherr, E. Rost, and M. E. Rickey, Phys. Rev. Letters 12, 420 (1964).

[10]Prakash and Austern do not give the absolute normalization of their form factor itself. Instead they give the absolute cross section of a DWBA (p,d) calculation that uses this form factor. We do not feel confident that we can reproduce their DWBA calculation, including all the correct multiplicative factors, in order to obtain the absolute normalization of their form factor.

[11]N. Austern, Phys. Rev. 136, 1743 (1964).

[12]W. T. Pinkston and G. R. Satchler, Nucl. Phys. 72, 641 (1965).

[13]B. F. Bayman and A. Kallio, Phys. Rev. 156, 1121 (1967).

[14]R. Jaffe and W. Gerace, Nucl. Phys. 125, 1 (1969).

[15]G. Bassani, N. Hintz, and C. D. Kovaloski, Phys. Rev. 136, B1006 (1964).

[16]J. C. Hafele, E. R. Flynn, and A. G. Blair, Phys. Rev. 155, 1238 (1967).